Supplement of SOIL, 11, 381–388, 2025
https://doi.org/10.5194/soil-11-381-2025-supplement

Supplement of

Calcium is associated with specific soil organic carbon decomposition products

Mike C. Rowley et al.

Correspondence to: Mike C. Rowley (mike.rowley@geo.uzh.ch)

SI Table of Contents

Fig. S1 – Total Ca concentrations of samples taken at the Forest and Grassland, California.

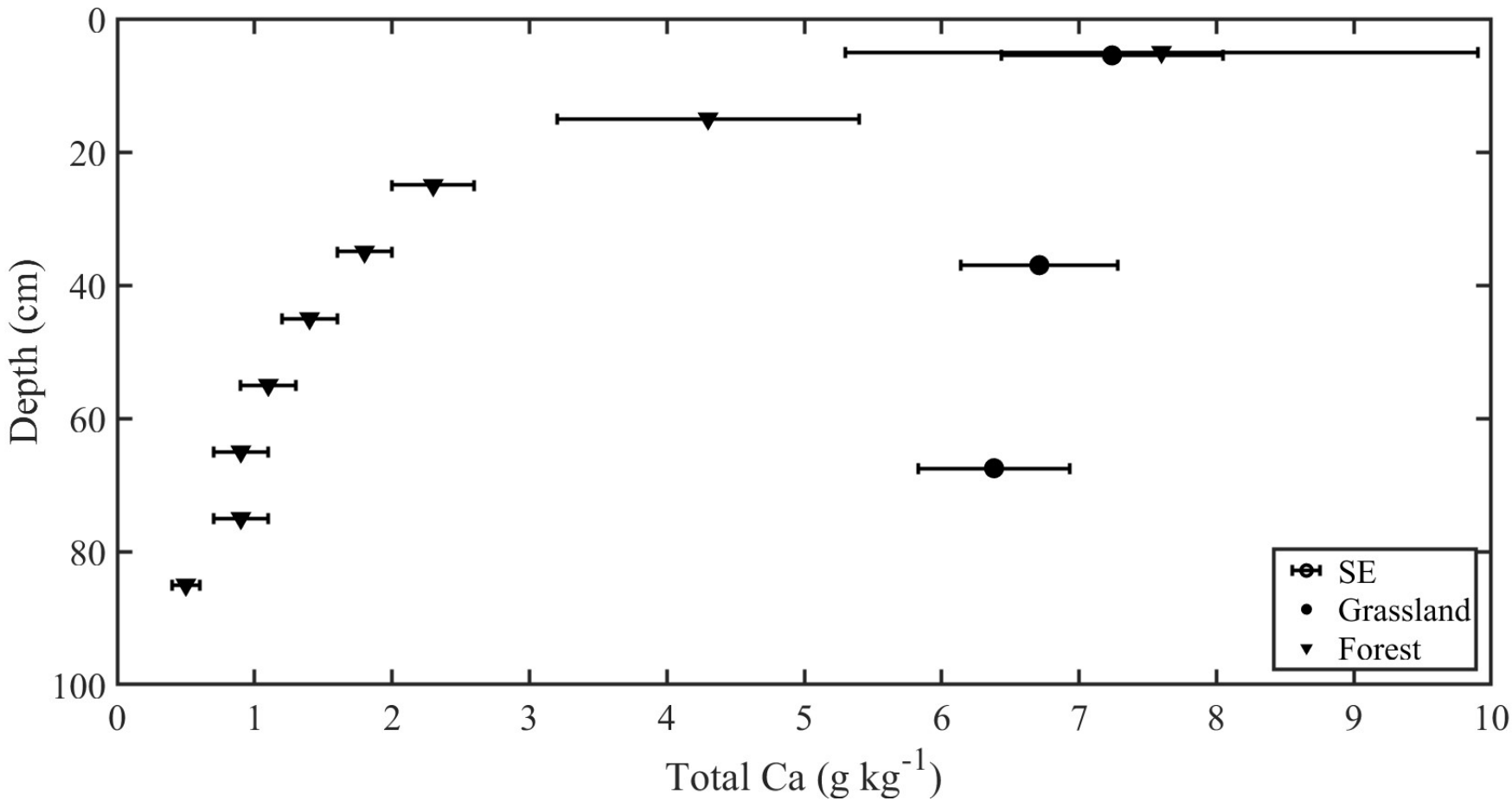

Fig. S1. Total Ca concentrations (g kg^{-1}) of soils from Blodgett (Forest) and Point Reyes (Grassland), California. Forest soil total contents were attained with X-ray fluorescence, while the Grassland samples were prepared with a lithium tetraborate fusion, forming pellets, which were subsequently dissolved in a weak acid, and then measured for total contents using inductively coupled plasma-atomic emission spectroscopy. The standard error of 6 soil core / replicates for the Forest (control and warmed plots 1-3) and 3 Grassland replicates are plotted as error bars horizontally behind the data.

Fig. S2 – Bulk soil properties at the Forest.

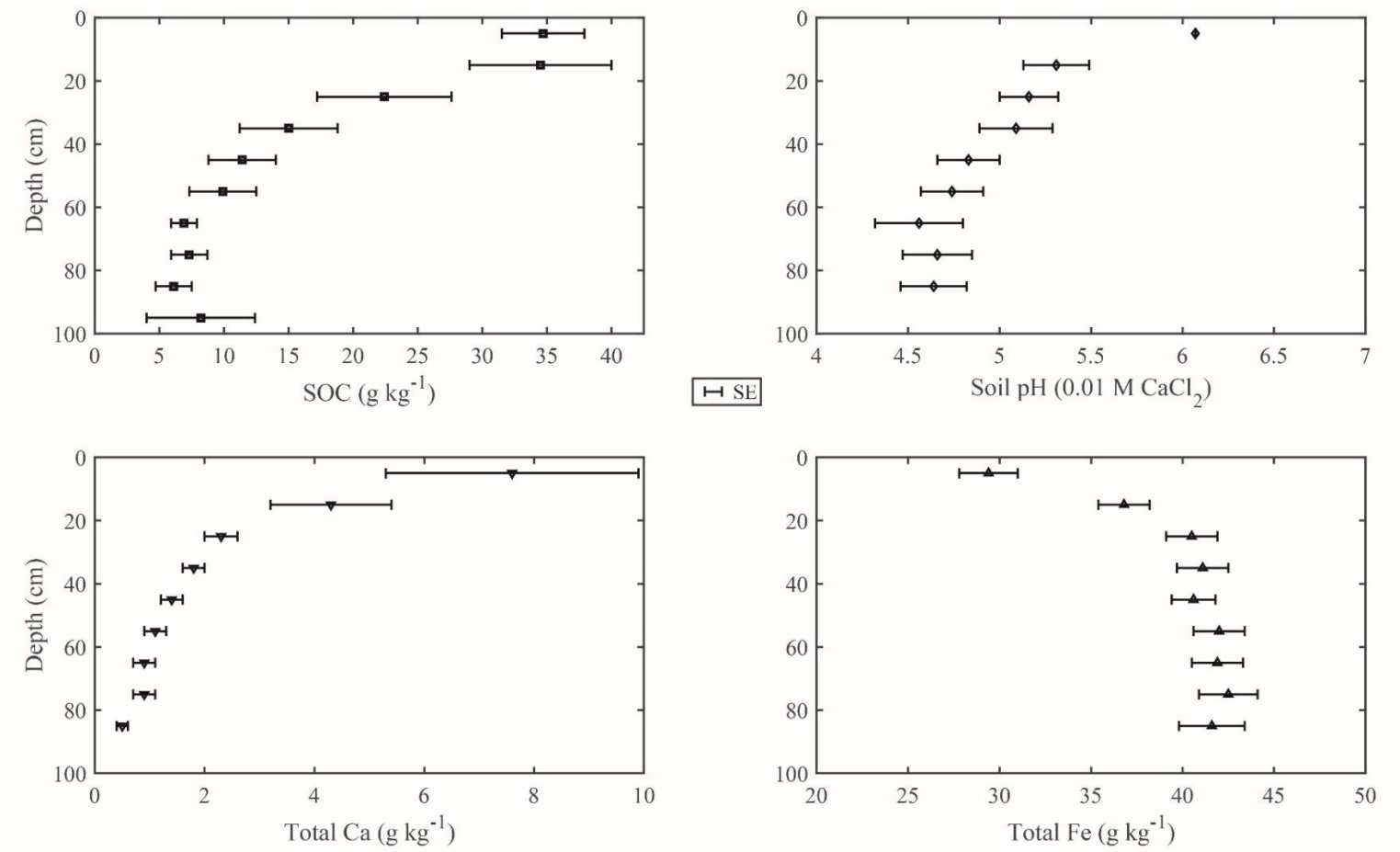

Fig. S2. Bulk soil properties at Blodgett site (Forest) averaged over the 6 soil core samples taken in 2018 from control and warmed paired plots 1-3 where the data is available (see table S1) with the standard error plotted as an error bar horizontally behind the data point. Soil organic carbon (g kg^{-1}) was ascertained with an elemental analyser. Soil pH was measured potentiometrically in 0.01 M $CaCl_2$. Total Ca and Total Fe (g kg^{-1}) were ascertained with X-ray fluorescence.

Fig. S3 – Map of California with sampling locations.

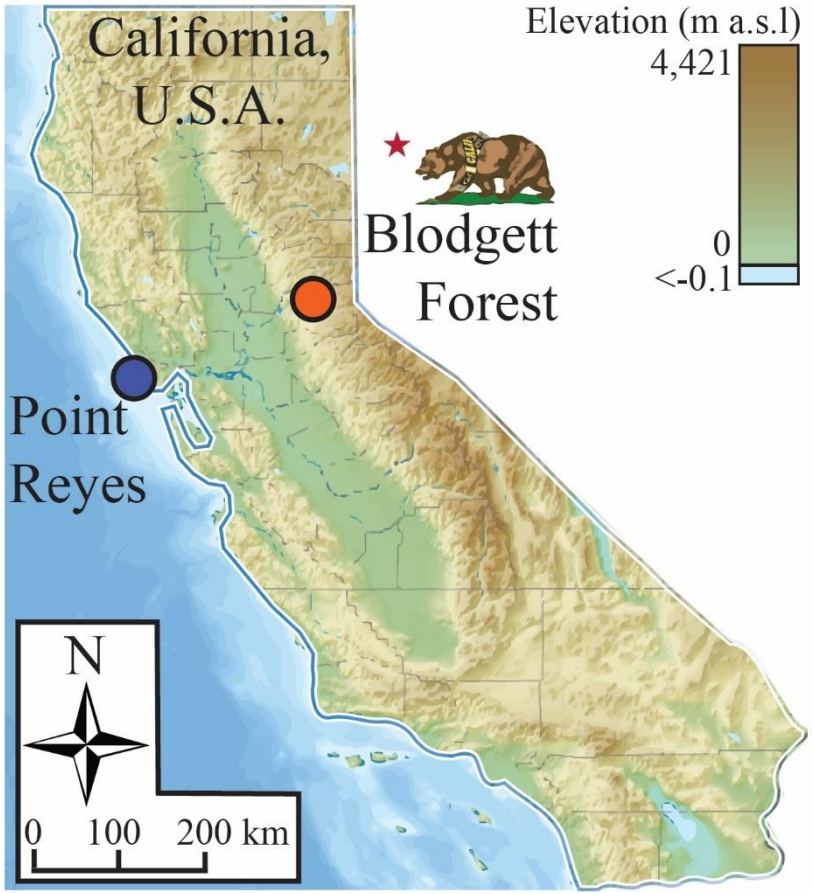

Fig. S3. Approximate locations of sampling sites in California for more details on the Blodgett site (Forest) see Hicks-Pires et al.[1] , while see Rowley et al.[2] for more details on Point Reyes (Grassland). The topographic map is adapted from ESRI[3]

Fig. S4 – Respiration data from different incubation experiments on the Forest samples.

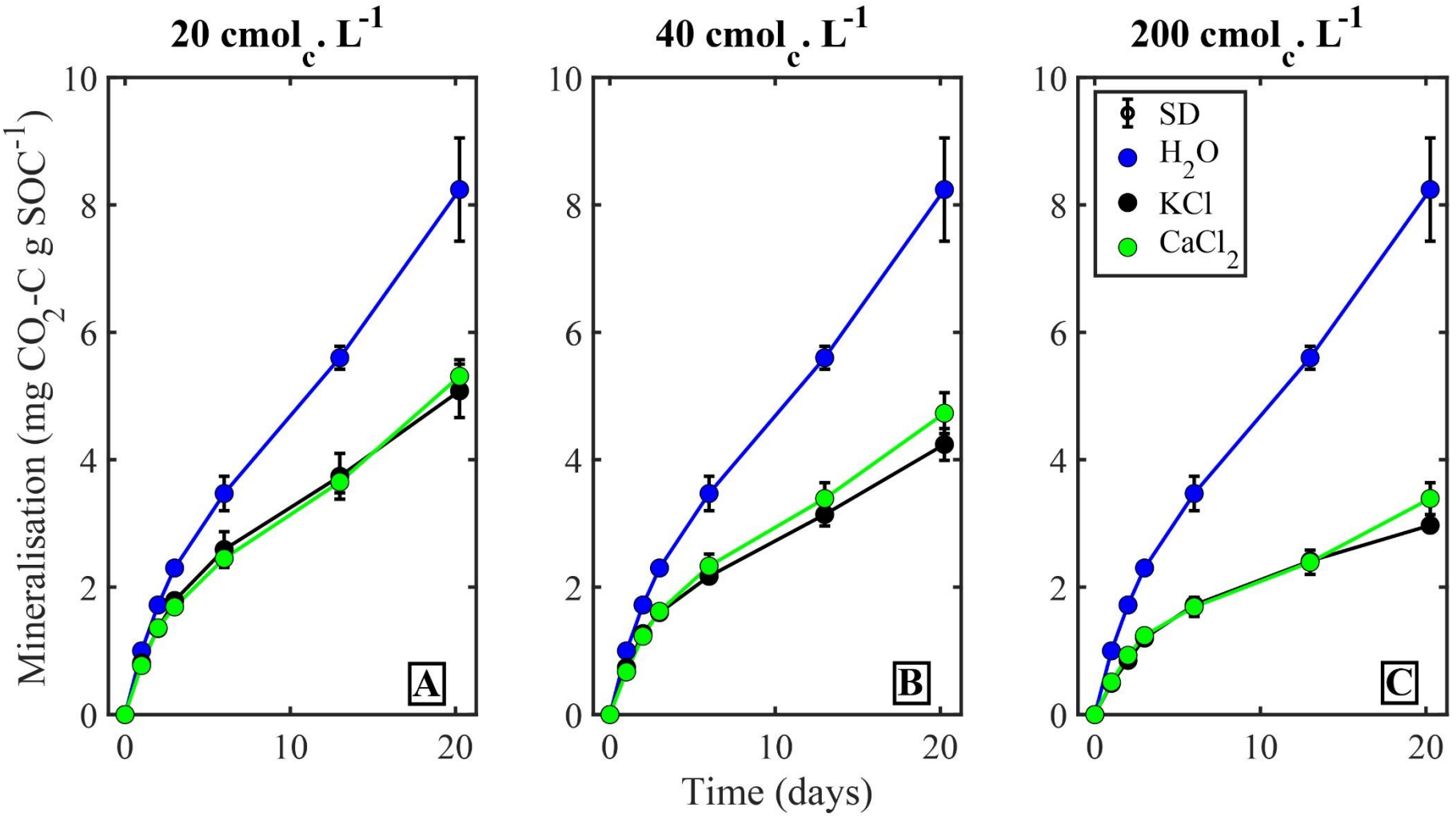

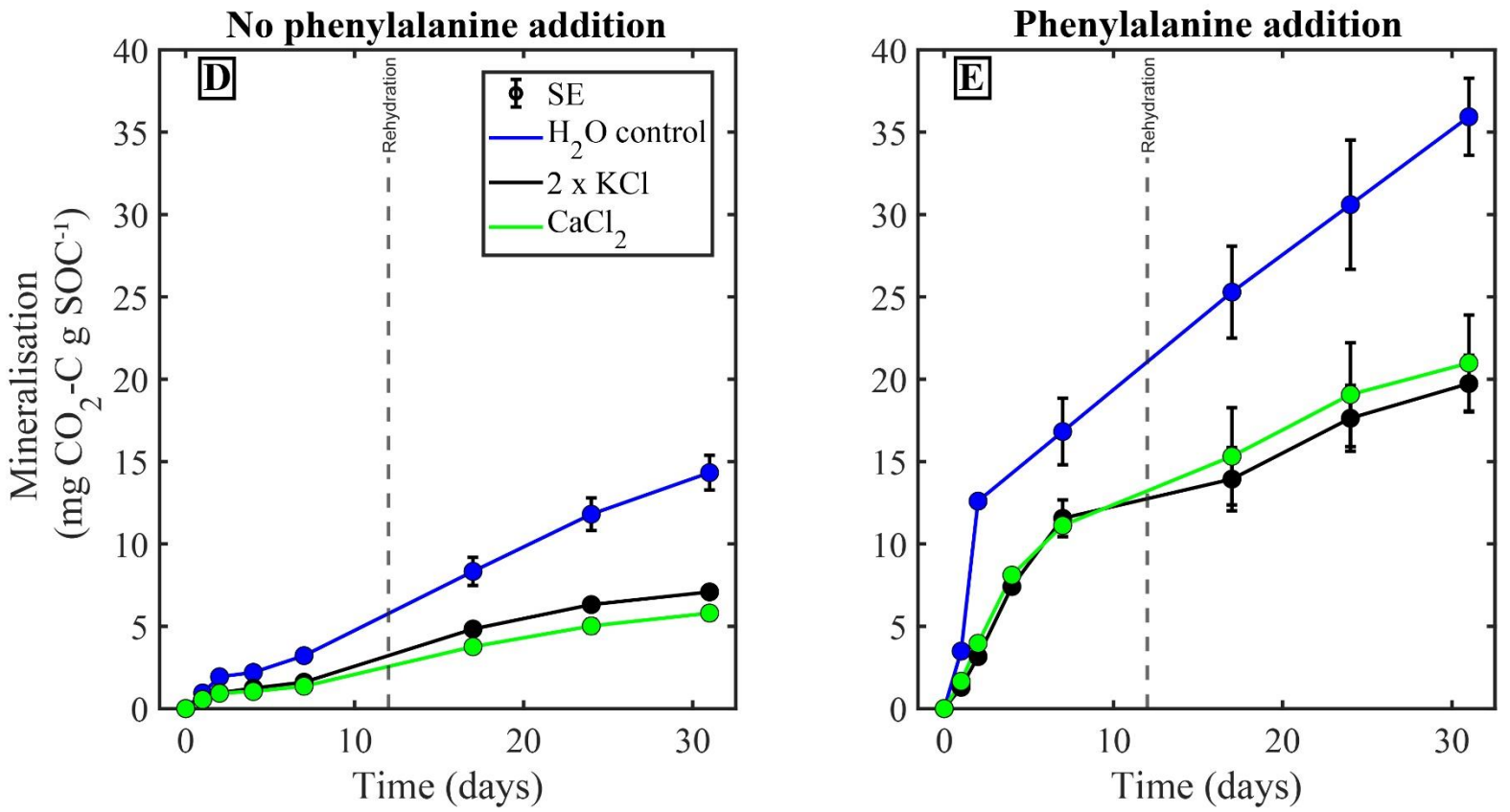

Fig. S4A. Respiration data in mineralised C (mg CO_2-C g SOC^{-1}) for different incubation experiments all run in duplicate on surface soil samples from the Blodgett site (Forest). A.) We tested the effect of increasing Ca or K addition on C mineralisation showing that increasing ionic strength or addition of Ca / K decreased the mineralisation of C, relative to the control. 20 centimoles of charge L^{-1} Ca or K ($c.mol_c$. L^{-1} or 0.1 M $CaCl_2$ or 0.78 g kg^{-1} Ca^{2+} / 0.2 M KCl or 1.52 g kg^{-1} K^+). **B.)** 40 centimoles of charge L^{-1} ($c.mol_c$. L^{-1} or 0.2 M $CaCl_2$ or 1.56 g kg^{-1} Ca^{2+} / 0.4 M KCl or 3.05 g kg^{-1} K^+). **C.)** 200 centimoles of charge L^{-1} ($c.mol_c$. L^{-1} or 1 M $CaCl_2$ or 7.81 g kg^{-1} Ca^{2+} / 2 M KCl or 15.23 g kg^{-1} K^+). **D.)** We then tested the influence C addition with phenylalanine (priming) and rehydration (birch effect) on 20 g of sample with either H_2O, $CaCl_2$ or 2 x KCl addition. Samples were incubated with a H_2O control or 140 centimoles of charge L^{-1} Ca or K ($c.mol_c$. L^{-1} or 0.7 M $CaCl_2$ or 5.61 g kg^{-1} Ca^{2+} / 1.4 M KCl or 11.04 g kg^{-1} K^+). **E.)** Samples were again incubated with a H_2O control or 140 centimoles of charge L^{-1} Ca or K, but this time also with the addition of phenylalanine at 6.3 % of the existing carbon content (0.7 M C or 1.75 g kg^{-1} C).

Fig. S5 – Aboveground biomass and litter STXM C NEXAFS measurements at the Forest.

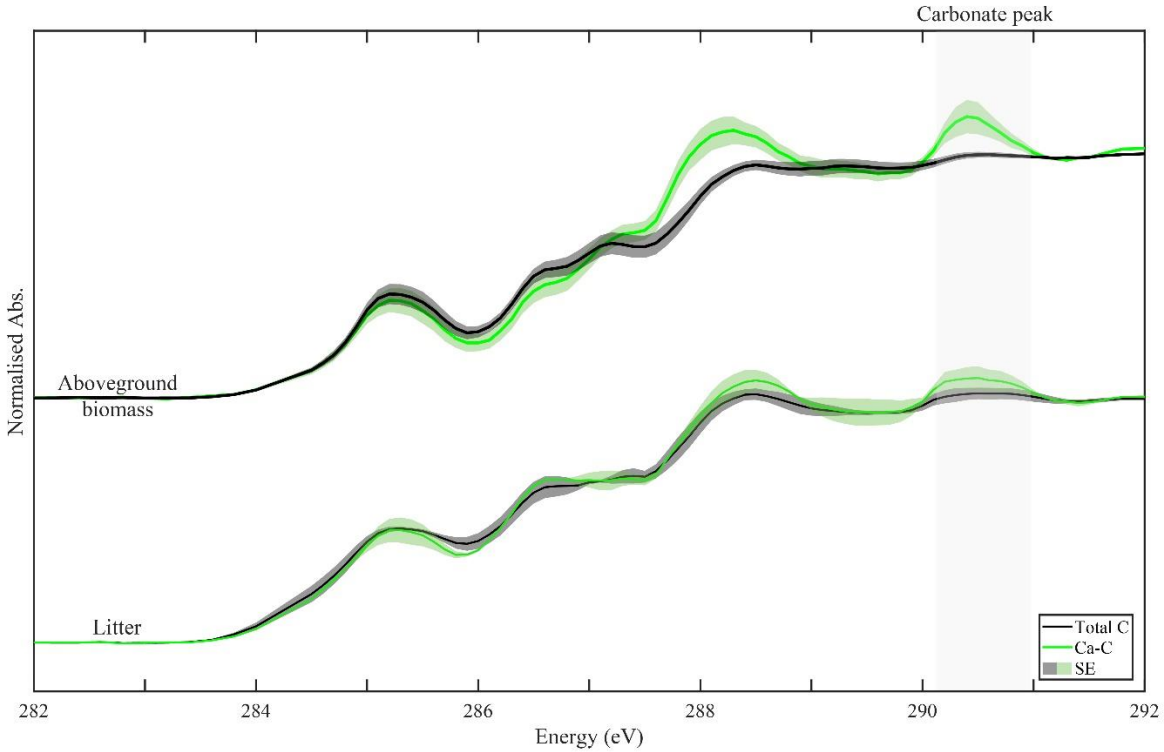

Fig. S5. The STXM C NEXAFS spectrum of carbon and the carbon associated with calcium in plant (leaf and branch mixed – aboveground biomass) and litter samples taken from Blodgett site (Forest) in January 2023. Importantly, the STXM C NEXAFS measurements of the aboveground biomass and litter sampled from the Forest had **a similar C speciation whether the spectra were associated with calcium or not**. As was discovered at Point Reyes (Grassland) there was little difference between the Ca-C and total C of aboveground biomass and soil samples. There was a slightly higher abundance in the carboxylic region (centred on 288.8 eV) and also a peak in the carbonate region (290.5 eV) in C associated with Ca in the aboveground biomass at the Forest (explored further below). Thus, the specific calcium-carbon association was not inherited from the biomass at the Forest and instead must have formed through a soil biogeochemical transformation process or processes. **The carbonate peak** (290.5 eV) could be related to a recent prescribed burn near the sampling site at the Forest prior to sampling, depositing carbonate aerosol (wood-fire stone) on the soil surface and vegetation, which was otherwise absent from the acidic soils developed in sedimentary deposits at the Grassland. This peak also corresponded with a slightly elevated soil pH in the surface of some samples (Table S1) but could not be verified on a bulk soil level during reaction with 10 % HCl. It could also be related to other biogenic processes.

Fig. S6 – Comparison of Grassland and Forest STXM C NEXAFS data of carbon in different elemental associations.

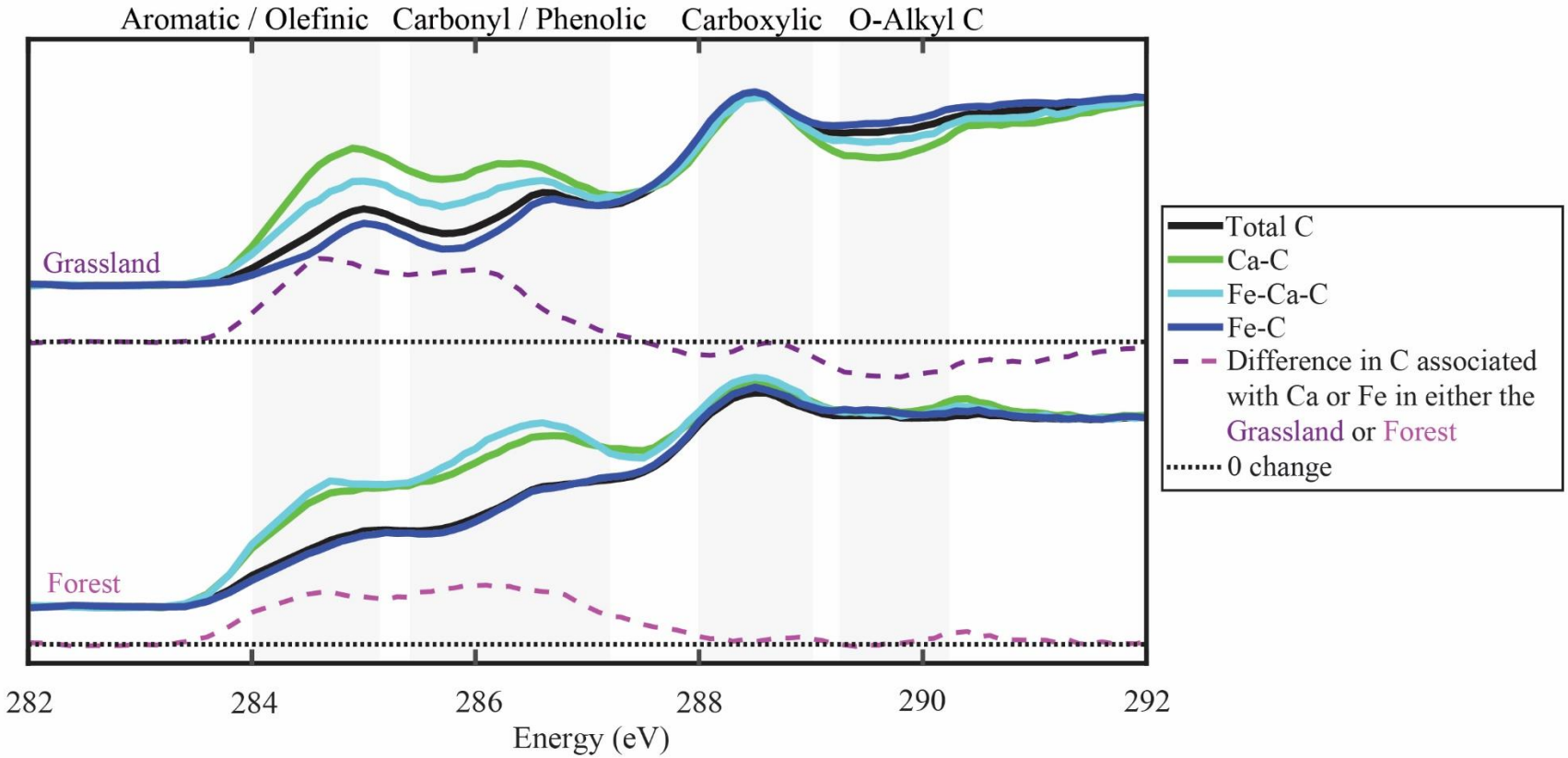

Fig. S6. Comparison of Point Reyes (Grassland)[2] and Blodgett (Forest), California scanning transmission X-ray microscope C near-edge X-ray absorption fine structure spectra, whereby C is separated by its co-location with different elements and then compared. Total / overall C (black), C associated with Ca, Fe and Ca, or with Fe in soils sampled from 3 depth intervals at the Grassland (*ca.* 0-10, 30-40, 60-70 cm) and Forest (10-20, 40-50 and 60-70 cm). The difference between the Ca-C and Fe-C is plotted as a dashed line under the data, while a 0-change reference plotted as a dotted line alongside the difference spectrum in black. The regions of the C_{1s} NEXAFS spectra that correspond to specific C functional groups or bonding environments are highlighted in grey boxes behind the spectra, with the corresponding text above the graph and were identified according to Lehmann, et al. [4].

Fig. S7 – Non-negative matrix factorisation end-member component spectra from the Forest soil core 3 sample taken from the 10-20 cm depth interval.

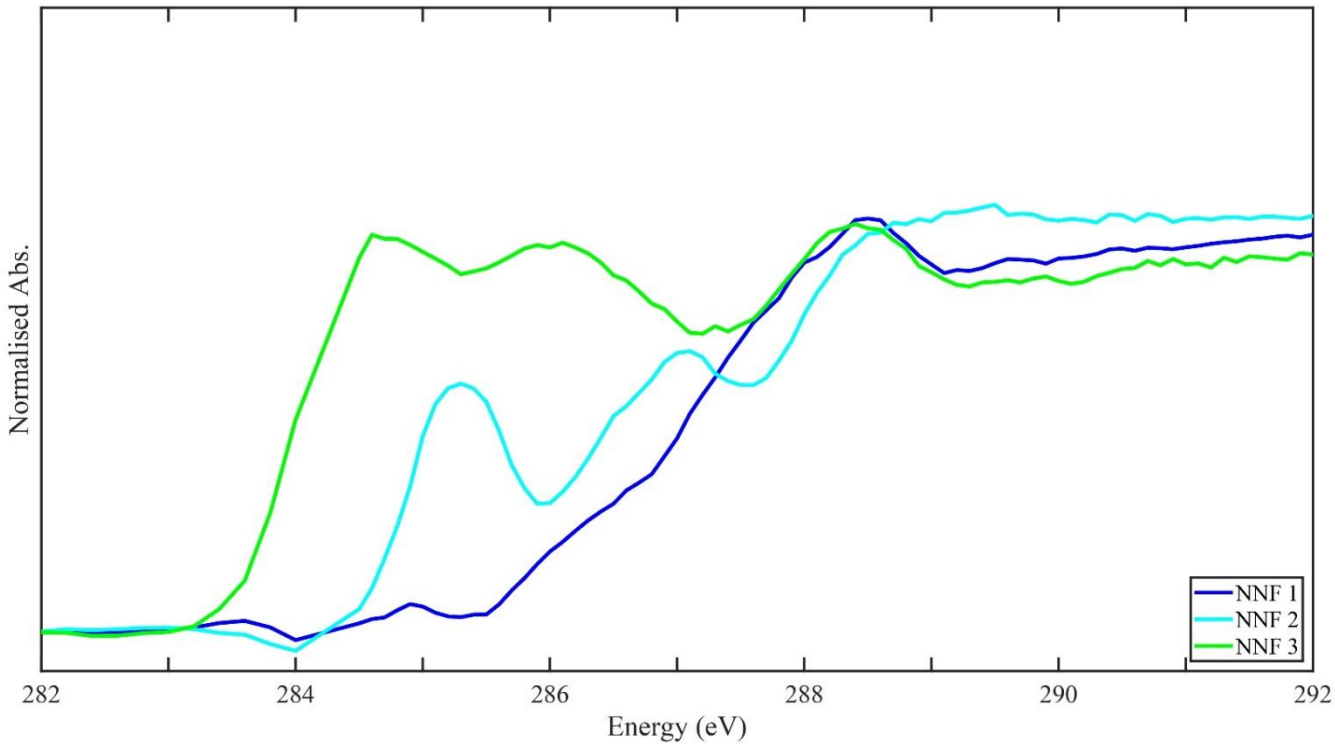

Fig. S7. Non-negative matrix factorisation component spectra from the control soil core 3 sample taken from the 10-20 cm depth interval at Blodgett (Forest), which were fit in Fig. 1B. The C in each stack was first separated with a Boolean function, grouped with principal component analysis, clustered with cluster analysis, and then grouped into spectral end-members using non-negative matrix factorisation analysis. Standard spectra associated with significant end-members were then fit to the whole stack with a least-squares means fit (without a Boolean defined mask), which gave the distribution of clusters presented in Fig. 1B. The relationship between NNF 1 and Fe explained 51.3 % of the variance (R^2 = 0.513, F(1, 11913) = 12558.9, p < 0.0001), C and NNF2 explained 60.6 % of the variance (R^2 = 0.606, F(1, 11021) = 16932.5, p < 0.0001), Ca and NNF 3 also explained 60.6 % of the variance (R^2 = 0.606, F(1, 11031) = 16949.6, p < 0.0001) in the soil core 3 sample example.

Fig. S8 – Tricolour concentration maps of the Forest soil core 4 (warmed plot 1) sample taken from between 60-70 cm before and after exchange with potassium (K) and then subsequent calcium (Ca) addition.

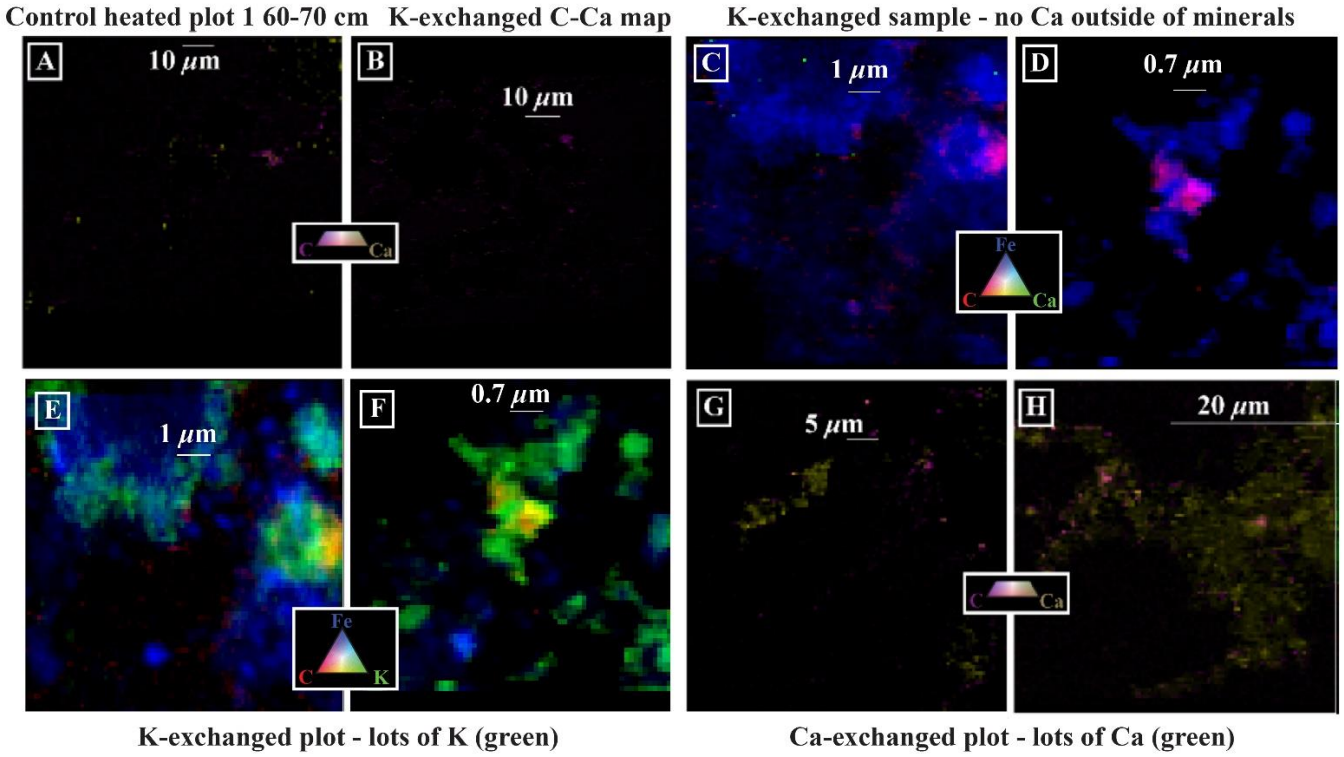

Fig. S8. Tricolours of extraction samples, control, K exchanged, Ca addition of soil core 4 (warmed plot 1) sample taken from 60-70 cm at Blodgett (Forest). A.) 100 x 100 μm Ca C map of the original sample **(control)** prior to extraction. **B.)** 100 x 100 μm **K exchanged sample**, remaining Ca is associated with mineral bodies **C & D**.) **K exchanged** stacks where Ca has been removed. **E & F.) The same K exchanged** samples, where instead of Ca being plotted in green, K was mapped above and below its L-edge to map K content of the samples, which was then plotted in green, demonstrating that the Ca has been replaced with K. **G & H.) Ca addition** samples, post K-exchange, where Ca (in yellow) has associated with available surfaces including remaining C and minerals.

Fig. S9 – STXM C NEXAFS spectra from the cation-exchange and incubation experiments on the Forest. samples.

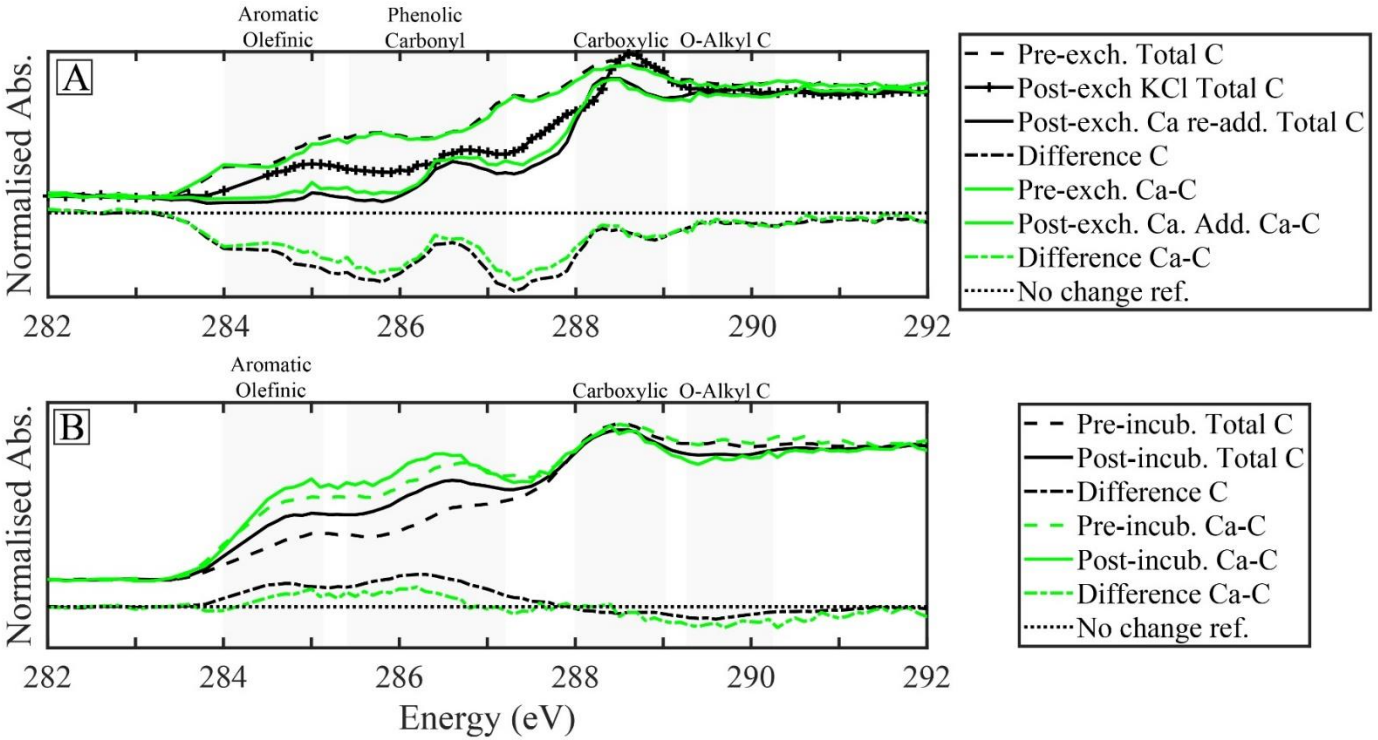

Fig. S9. The scanning transmission X-ray microscope carbon near-edge X-ray absorption fine structure (STXM C NEXAFS) spectra from the cation-exchange and incubation experiments completed on the surface soil samples from the Blodgett (Forest) site. A.) The total carbon and calcium-carbon STXM C NEXAFS spectra of samples taken from the surface of the Forest before and after extraction with potassium (KCl) and then, after the addition of calcium ($CaCl_2$) to potassium-exchanged samples, there was no calcium left associated with carbon after potassium exchange. The calcium-carbon and total carbon signal were separated using techniques explored in Rowley et al.[2] **B.)** STXM C NEXAFS spectra of the incubated samples. Incubation after calcium addition increases both the calcium-carbon signal and the relative aromatic and phenolic carbon contents of total carbon, reproducing the calcium-carbon signal of unaltered samples, while decreasing the O-alkyl carbon peak location.

Fig. S10 – Conceptual model of Ca-C interactions within the decomposition continuum.

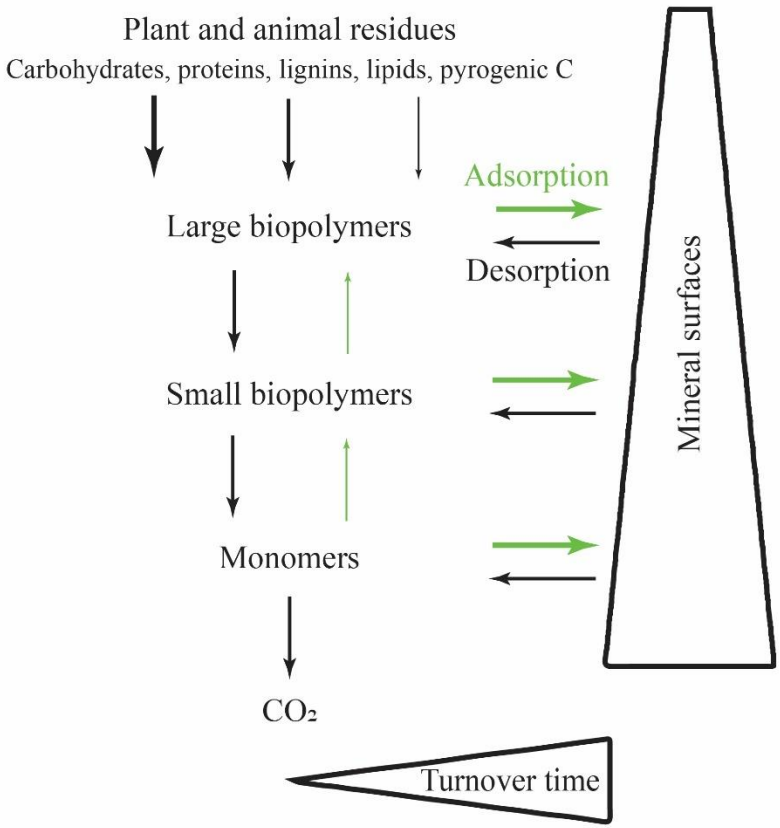

Fig. S10 – Conceptual model of the interactions between calcium and carbon adapted from and inspired by the Decomposition Continuum model of Lehmann and Kleber[5]. The role of calcium in the decomposition continuum has been highlighted in green, whereby decomposition along the continuum increases the propensity of carbon for binding and co-location with calcium by decreasing the size of biopolymers, while increasing the relative proportions of functional groups. This binding by calcium can link different biomolecules, increasing their relative size as they move through the continuum, but not forming new molecules (like with condensation). Speculatively this organo-metal-organic binding is happening to a lesser degree and thus has smaller arrows. While calcium can influence aggregation, this has been left out of this diagram to focus on our observations within this study.

Table S1 – Bulk soil properties of the Forest samples.

Table S1. Bulk soil properties for soil core 1-6 at Blodgett Forest. Elemental analysis was completed on soil cores from the same sampling campaign as the initial STXM C NEXAFS analyses (2021), while X-ray fluorescence and soil pH analyses were completed on samples from the same experimental plots, sampled in 2018. Soil pH was recorded as part of Zosso et al.[6] where averages have been presented previously. -*indicates where data is unavailable.

Treatment	Soil core	Depth	Elemental analyser			Soil pH	XRF (g kg^{-1})										
		(cm)	C (g kg^{-1})	N (g kg^{-1})	C:N Ratio	0.01 M $CaCl_2$	Ca	Fe	Na	Mg	Al	Si	P	S	K	Ti	Mn
Control plots (1-3)	1	0-10	27.6	1.1	25.8	-*	2.8	34.9	8.9	7.9	117.7	184	0.8	0.3	18	4.5	1.4
	1	10-20	40.5	1.4	28.5	5.1	2.2	42.7	9	9.3	138.2	165.2	0.8	0.3	17.9	5.3	2.1
	1	20-30	16.0	0.7	22.9	5.0	1.9	44.5	7.9	9.3	144.8	167.9	0.4	0.3	18.2	5.6	1.3
	1	30-40	8.9	0.5	18.6	4.8	1.8	45.8	6.8	9	146.9	173.7	0.3	0.2	18.7	5.6	0.5
	1	40-50	8.0	0.5	15.7	4.5	1.4	44	7.2	8.8	142.7	175.9	0.3	0.2	18.9	5.7	0.4
	1	50-60	6.7	0.5	12.5	4.7	0.9	45.7	6.9	8	145.6	180.3	0.2	0.2	19	5.2	0.2
	1	60-70	7.3	0.5	15.5	4.5	0.8	44.9	5.9	7.8	143.4	181.7	0.2	0.2	19.6	5	0.2
	1	70-80	-*	-*	-*	4.3	1.3	42.7	7.2	8.1	136.3	181.4	0.2	0.2	19.9	5.1	0.2
	1	80-90	2.8	0.3	8.1	4.3	0.3	47.2	5.6	7.3	151.6	175.6	0.2	0.3	19.9	5.1	0.2
	1	90-100	1.6	0.4	4.5	-*	-*	-*	-*	-*	-*	-*	-*	-*	-*	-*	-*
	2	0-10	41.0	1.5	27.7	-*	5.2	29.2	8.4	6.7	93.8	211.8	0.7	0.6	19.2	3.8	0.9
	2	10-20	46.4	1.4	32.1	5.1	3.8	38.2	9.7	8.5	134.1	174.5	1	0.4	18.8	5.1	1.5
	2	20-30	32.3	1.2	25.8	5.1	2.5	35.8	7.7	8.7	133.6	181.3	0.6	0.3	17.8	4.8	2
	2	30-40	21.1	1.0	21.7	4.8	1.6	39.8	8.1	8.6	139.3	183.4	0.3	0.4	18.7	5.2	0.7
	2	40-50	10.9	0.6	19.2	4.6	1.3	38.1	6.8	8.3	144.6	194.7	0.2	0.3	18.7	5.1	0.3
	2	50-60	7.2	0.6	12.6	4.3	1.1	38.2	7.1	8	144.3	197.8	0.2	0.2	18.7	4.9	0.2
	2	60-70	9.0	0.5	17.4	4.3	0.9	38.9	5.9	7.7	139.4	197.2	0.2	0.2	18.5	5	0.2
	2	70-80	10.4	0.6	18.0	4.2	0.9	38.7	6.4	7.8	141.2	195.8	0.2	0.2	18.3	4.8	0.2
	2	80-90	10.6	0.6	17.2	4.4	0.7	36.8	6.4	8	143.5	201.6	0.1	0.2	18.4	4.5	0.2
	2	90-100	8.2	0.3	23.4	-*	-*	-*	-*	-*	-*	-*	-*	-*	-*	-*	-*
	3	0-10	25.7	1.1	23.7	6.1	10.2	30.6	8.1	8.8	102.3	199.6	1.7	0.4	19.7	4.1	2.1
	3	10-20	13.5	0.6	22.7	6.2	4.8	35.9	7.7	9	132.4	200.5	0.4	0.2	20	4.8	1.5
	3	20-30	7.7	0.5	14.2	5.9	3.6	38.7	8	9.4	139.9	181.6	0.3	0.2	19.7	5	1
	3	30-40	5.2	0.4	12.4	5.8	2.9	37.3	6.8	8.7	139.4	189.1	0.2	0.2	19	5.1	0.7
	3	40-50	3.9	0.4	10.5	5.7	2.5	36.9	7	8.4	137.1	201	0.1	0.1	19.6	4.7	0.4
	3	50-60	4.4	0.4	12.1	5.6	2	37.2	6.5	8.6	136.8	203.6	0.1	0.1	19.5	4.7	0.3
	3	60-70	3.4	0.4	8.5	5.6	1.9	36.2	6.2	8.8	135	217.6	0.1	0.2	20.6	4.7	0.2
	3	70-80	2.2	0.4	5.2	5.6	1.5	38.2	6.7	8.9	144.5	227.8	0.2	0.2	21.4	4.8	0.2
	3	80-90	2.4	0.3	8.0	5.6	1.1	37	6.1	8.6	142.3	230.5	0.2	0.2	21.9	4.4	0.2
	3	90-100	2.3	0.4	5.1	-*	-*	-*	-*	-*	-*	-*	-*	-*	-*	-*	-*

Warmed plots (1-3)	4	0-10	-*	-*	-*	-*	19.4	23.0	10.9	6.7	64.1	155.4	2.2	0.7	13.4	2.8	1.7
	4	10-20	52.4	1.2	43.1	5.5	9.8	34.5	9.7	8.7	115.3	150.0	1.8	0.3	17.3	4.6	1.7
	4	20-30	45.3	0.8	54.7	5.4	1.9	45.6	7.8	8.4	146.2	173.9	0.4	0.2	20.7	5.7	0.9
	4	30-40	32.6	0.7	48.4	5.7	1.4	46.0	7.6	8.3	145.5	174.0	0.3	0.2	22.0	5.7	0.5
	4	40-50	24.5	0.8	31.9	5.0	1.2	45.4	7.4	8.2	143.9	176.4	0.3	0.2	23.4	5.5	0.3
	4	50-60	14.9	0.7	22.7	4.9	1.0	46.1	6.5	8.0	146.4	180.1	0.3	0.2	24.5	5.4	0.3
	4	60-70	9.0	0.4	25.4	4.8	0.7	45.5	7.0	7.5	146.3	177.9	0.3	0.2	25.0	5.2	0.3
	4	70-80	7.8	0.6	14.1	4.8	0.4	49.7	7.2	7.1	151.3	164.7	0.4	0.2	27.1	5.6	0.3
	4	80-90	8.5	0.5	16.8	4.7	0.4	45.8	7.5	6.9	144.3	174.3	0.4	0.2	29.9	5.1	0.3
	4	90-100	26.4	0.5	54.4	-*	-*	-*	-*	-*	-*	-*	-*	-*	-*	-*	-*
	5	0-10	44.1	1.7	26.7	-*	3.6	26.2	7.5	6.2	83.7	261.9	0.5	0.4	18.2	3.4	1.2
	5	10-20	30.0	1.4	21.9	4.9	2.6	31.6	7.8	7.1	102.0	213.2	0.4	0.3	21.6	4.2	1.3
	5	20-30	19.6	0.9	23.0	4.9	2.1	40.1	7.6	9.0	138.5	179.2	0.4	0.3	20.3	5.3	0.8
	5	30-40	11.1	0.6	19.2	4.7	1.5	39.7	6.0	8.8	138.3	185.1	0.3	0.2	21.8	5.3	0.4
	5	40-50	10.0	0.7	14.9	4.5	1.0	39.7	7.8	8.5	137.1	193.6	0.2	0.2	23.4	5.2	0.3
	5	50-60	21.7	0.5	46.2	4.4	0.7	42.9	6.6	8.1	139.4	190.6	0.2	0.2	24.3	5.4	0.3
	5	60-70	-*	-*	-*	3.7	0.7	43.9	7.1	8.0	138.1	186.6	0.2	0.2	25.8	5.4	0.2
	5	70-80	10.4	0.4	29.2	4.6	0.6	44.1	7.7	8.2	140.2	186.8	0.2	0.2	27.3	5.5	0.2
	5	80-90	9.3	0.5	19.5	4.5	0.5	44.8	7.2	8.5	137.9	184.6	0.3	0.2	28.1	5.5	0.3
	5	90-100	-*	-*	-*	-*	-*	-*	-*	-*	-*	-*	-*	-*	-*	-*	-*
	6	0-10	35.0	1.5	23.1	-*	4.6	32.6	9.0	8.8	118.3	195.6	0.6	0.5	18.7	4.4	1.4
	6	10-20	24.0	1.1	22.4	5.0	2.7	38.0	9.1	9.6	138.6	192.1	0.4	0.3	19.9	5.0	1.0
	6	20-30	13.6	0.6	21.0	4.7	1.6	38.3	8.7	9.5	144.2	205.4	0.3	0.3	20.0	5.2	0.6
	6	30-40	11.2	0.6	17.5	4.7	1.6	38.0	8.0	9.2	141.2	210.7	0.2	0.2	20.2	5.0	0.4
	6	40-50	11.0	0.6	19.1	4.7	1.3	39.7	7.2	9.1	144.9	219.9	0.2	0.2	19.6	5.3	0.4
	6	50-60	4.6	0.4	11.4	4.6	0.6	41.7	7.1	8.1	148.7	219.4	0.2	0.2	18.2	4.9	0.2
	6	60-70	5.7	0.5	11.2	4.5	0.3	42.1	6.4	7.9	155.9	218.6	0.2	0.3	17.0	4.5	0.2
	6	70-80	5.7	0.4	13.4	4.4	0.5	41.5	6.7	8.4	153.1	219.7	0.2	0.3	17.8	4.6	0.2
	6	80-90	2.8	0.4	7.1	4.4	0.3	38.2	6.5	8.6	151.4	228.5	0.1	0.3	16.1	4.1	0.2
	6	90-100	2.3	0.3	6.9	-*	-*	-*	-*	-*	-*	-*	-*	-*	-*	-*	-*

Table S2. Linear mixed-effects model results – incubations with increasing Ca content.

Linear mixed-effects model fit by ML

Model information: Number of observations: 98; Fixed effects coefficients: 14; Random effects coefficients 9; Covariance parameters 3

Formula: Mineralization ~ 1 + Time*Treatment + (1 | Replication) + (1 | Time)

Model fit statistics:			
AIC	**BIC**	**LogLikelihood**	**Deviance**
136.86	180.81	-51.431	102.86

Fixed effects coefficient (95% Cis)							
Name	**Estimate**	**SE**	**tStat**	**DF**	**pValue**	**Lower**	**Upper**
(Intercept)'	0.74254	0.23339	3.1816	84	0.0020533	0.27842	1.2067
Time'	0.37883	0.023544	16.09	84	2.19E-27	0.33201	0.42565
Treatment_CaCl20'	-0.10169	0.19112	-0.53207	84	0.59608	-0.48175	0.27837
Treatment_KCl20'	-0.01703	0.19112	-0.08909	84	0.92922	-0.39709	0.36304
Treatment_CaCl40'	-0.11871	0.19112	-0.62113	84	0.5362	-0.49877	0.26135
Treatment_KCl40'	-0.06594	0.19112	-0.34501	84	0.73095	-0.446	0.31412
Treatment_CaCl200'	-0.26154	0.19112	-1.3684	84	0.17482	-0.6416	0.11852
Treatment_KCl200'	-0.0531	0.19112	-0.27784	84	0.78182	-0.43316	0.32696
Time:Treatment_CaCl20'	-0.14162	0.020161	-7.0244	84	5.22E-10	-0.18171	-0.10153
Time:Treatment_KCl20'	-0.1514	0.020161	-7.5096	84	5.76E-11	-0.19149	-0.11131
Time:Treatment_CaCl40'	-0.16661	0.020161	-8.264	84	1.79E-12	-0.2067	-0.12652
Time:Treatment_KCl40'	-0.19278	0.020161	-9.5623	84	4.39E-15	-0.23287	-0.15269
Time:Treatment_CaCl200'	-0.22904	0.020161	-11.361	84	1.16E-18	-0.26914	-0.18895
Time:Treatment_KCl200'	-0.30482	0.020161	-15.12	84	1.08E-25	-0.34492	-0.26473

Supplementary methods:

Sampling and bulk characterisation: The bulk soil X-ray fluorescence data and soil pH values were measured on soil core samples taken in April 2018. Samples were bagged in the field and transported to Lawrence Berkeley National Laboratory for further analysis. The samples sent to UZH for XRF and soil pH were freeze-dried followed by terminal oven drying to a constant weight at 40°C. Total element contents were established using X-ray fluorescence (SPECTRO X-LAB 2000) without loss on ignition treatment, which through pre-testing was found to have negligible difference on the overall results.

Incubations: We tested the effect of different anions (Cl^- *vs.* SO_4^{2-}), different concentrations of $CaCl_2$ or KCl (Fig. S8A-C), the effect of glucose (not included) or phenylalanine addition, and rehydration during pretesting (Fig. S8D-E). In conclusion, both Cl^- *vs.* SO_4^{2-} had a similar effect on cumulative CO_2 production (data not shown), increasing ionic strength reduced mineralised CO_2-C, while carbon addition and rehydration increased CO_2 production due to the priming and Birch effect, respectively. Finally, the control, potassium-exchanged, calcium-addition, and calcium-addition incubated samples were analysed using STXM C NEXAFS. We calculated the significance (p value $\alpha = < 0.05$) of differences in our incubation data using a linear mixed-effects model with time point and replication unit set as repeated measures (Table S2).

STXM C NEXAFS - warming: Contrary to our initial hypothesis, any differences that did exist at the microscale from the control and warmed plots were driven by one specific depth interval (40-50 cm) and were small, relative to the effect of different elemental association.

References.

1 Hicks Pries, C. E., Castanha, C., Porras, R. C. & Torn, M. S. The whole-soil carbon flux in response to warming. *Science* **355**, 1420-1423 (2017). https://doi.org/10.1126/science.aal1319

2 Rowley, M. C. *et al.* Association between soil organic carbon and calcium in acidic grassland soils from Point Reyes National Seashore, CA. *Biogeochemistry* **165**, 91-111 (2023). https://doi.org/10.1007/s10533-023-01059-2

3 ESRI. World imagery "Sources: Esri, DigitalGlobe, GeoEye, i-cubed, USDA FSA, USGS, AEX, Getmapping, Aerogrid, IGN, IGP, swisstopo, and the GIS User Community" / National geographic "Sources: National Geographic, Esri, DeLorme, HERE, UNEP-WCMC, USGS, NASA, ESA, METI, NRCAN, GEBCO, NOAA, iPC" (ESRI, 2024).

4 Lehmann, J. *et al.* in *Biophysico-Chemical Processes Involving Natural Nonliving Organic Matter in Environmental Systems* (eds N. Senesi, B. Xing, & P. M. Huang) Ch. 18, 723-775 (John Wiley & Sons Inc., 2009).

5 Lehmann, J. & Kleber, M. The contentious nature of soil organic matter. *Nature* **528**, 60-68 (2015). https://doi.org/10.1038/nature16069

6 Zosso, C. U. *et al.* Whole-soil warming decreases abundance and modifies the community structure of microorganisms in the subsoil but not in surface soil. *SOIL* **7**, 477-494 (2021). https://doi.org/10.5194/soil-7-477-2021